Published by :
http://www.ijert.org

International Journal of Engineering Research & Technology (IJERT)
ISSN: 2278-0181
Vol. 6 Issue 01, January-2017

Influence of Cu Substitution on Physical Properties of Co-Zn Ferrite Nanoparticles

K. Rajasekhar Babu[1], M. Purnachandra Rao[1],
P. S. V. Subba Rao[1],
K. Rama Rao[1]
[1]Department of Physics, Andhra University,
Visakhapatnam, Andhra Pradesh

Abstract- **In this work, influence of Cu substitution on structural and magnetic properties of Cobalt-Zinc ferrite nanoparticles synthesized by sol-gel combustion method have been investigated. All the samples exhibit cubic spinel structure and the lattice constant decreases linearly with increasing Cu-content. Average crystallite sizes calculated from Debye-Scherrer formula are in the range of 51-100nm. Cation distribution estimated form X-ray line intensity calculations show that Cu ions simultaneously occupy tetrahedral (A) and octahedral (B) sites with different ratio and Zn and Co ions occupies A and B sites respectively. With increasing Cu content a fraction of Co ions migrate to A site when x>0.2. Saturation magnetization (Ms), Coercivity (Hc) and remanent magnetization (Mr) that varies significantly with Cu-Content. Saturation magnetization decreases from 90.7 emu/g (x=0.0) to 51 emu/g (x=0.4). The proposed cation distribution supports the variation in saturation magnetization and Coercivity with increasing Cu content.**

Keywords: Spinel Ferrite, Co-Zn Ferrite, Sol-Gel Combustion, XRD,

1. INTRODUCTION

Spinel ferrites are the promising ceramic magnetic materials, which have wide range of applications in various fields like electric, magnetic, electronics, microwave devices, catalysts, transformers cores, power conversions, high frequency applications in telecommunications, magnetically control drug delivery system, multilayer inductor applications. Recently tremendous importance has been given to nanoferrite particles due to their potential for elucidating fundamental nanomagnetism and technological applications in diverse fields.

The general chemical formula for cubic spinel ferrites is MFe_2O_4, where M is a divalent transition metal ion and Fe is a trivalent iron ion. The spinel lattice is composed of a closed packed arrangement of 32 oxygen ions leaving two kinds of interstitial sites: tetrahedral (A) and octahedral (B) site. The physical properties of these ferrites are very sensitive to the chemical composition, method of preparation, particle size, and micro structure and in particular density of cations in A and B sites [1]. Among the spinel ferrites, Cobalt and Zinc ferrites have attracted considerable interest because of their wide range of applications [2-5]. In case of bulk Co ferrite, Co^{2+} ions occupy mainly B-sites and Fe^{3+} ions are distributed equally in to both A and B sites, whereas Zn^{2+} ions prefer to occupy A-sites and Fe^{3+} ions are confined to B-sites only in Zn ferrite [2]. The substation of non-magnetic Zn^{2+} ions in place of ferromagnetic Co^{2+} ions results in the displacement of Fe^{3+} ions from B to A sites. Thus the redistribution of cations among A and B sites significantly alters the structural and magnetic properties.

The properties of Co-Zn ferrite can be improved by choosing a suitable dopant and synthesis method. Several authors reported that Copper ion containing ferrites exhibit novel magnetic properties [6-8]. The presence of copper ions at octahedral sites create John Teller distortion and affects the crystal field and acts as a relaxator, and decreases the dielectric loss. Under certain conditions like at high-temperature copper ferrite exhibits cubic phase and tetragonal phase in low-temperatures. Statistically, Cu ferrite crystallized in to inverse spinel structure in which 6-24% of Cu ions occupy A-sites depending on the method of preparation [9].

Even though many interesting works have been carried out on Cobalt-Zinc ferrite system, systematic investigation of Cu^{2+} doped Co-Zn ferrites are few. With this in mind, the present work aims to shed light on the influence of Cu^{2+} substitution on structural and magnetic properties of $Co_{0.5}Zn_{0.5-x}Cu_xFe_2O_4$ (x=0.0 to 0.4 insteps of 0.1) system synthesized via sol-gel combustion method.

2. EXPERIMENTAL DETAILS

A series of $Co_{0.5}Zn_{0.5-x}Cu_xFe_2O_4$ (x=0.0 to 0.4 insteps of 0.1) nanoparticles were prepared through Sol-gel combustion method. The stoichiometric amounts of A.R grade copper nitrate ($Cu(NO_3)_2.3H_2O$), zinc nitrate ($Zn(NO_3)_2.6H_2O$), cobalt nitrate ($Co(NO_3)_2.3H_2O$) and ferric nitrate ($Fe(NO_3)_3.9H_2O$) were dissolved in minimum amount of de-ionized water to get a clear solution. The molar ratio of citric acid to metal nitrates was taken as 1:3. The citric acid solution was mixed with metal nitrates solution and pH of the mixed metal nitrates solution was adjusted to 7 by adding a few drops of aqueous ammonia. Then the mixed solution was heated to transform into very viscous brown gel. After the evaporation of water molecules from the mixture, the gel began frothing and automatically ignited, burnt with glowing flints. The combustion reaction was completed within a few seconds and loose powders are formed. These powders were crushed, ground thoroughly and sintered at 1050^{o}C for 4 hrs in air atmosphere.

International Journal of Engineering Research & Technology (IJERT)
ISSN: 2278-0181
Vol. 6 Issue 01, January-2017

The X-ray diffraction measurements were carried out by X-ray diffractometer (PAN Analytical Xpert Pro) with Cu-Kα (λ=1.5406Å) radiation to ensure single- phase and the nature of the prepared samples. SEM images of as prepared samples were recorded using a Quanta 200 FEG scanning electron microscope (SEM). The magnetic measurements were made on Lakeshore VSM 7410 vibrating sample magnetometer.

3. RESULTS AND DISCUSSIONS

3.1 Lattice Constant and crystallite size

Fig. 1 shows the powder XRD patterns of the samples sintered at 1050°C for 4hr. All the peaks in the XRD patterns of the samples are due to the spinel lattice, indicating the absence of any secondary phase.

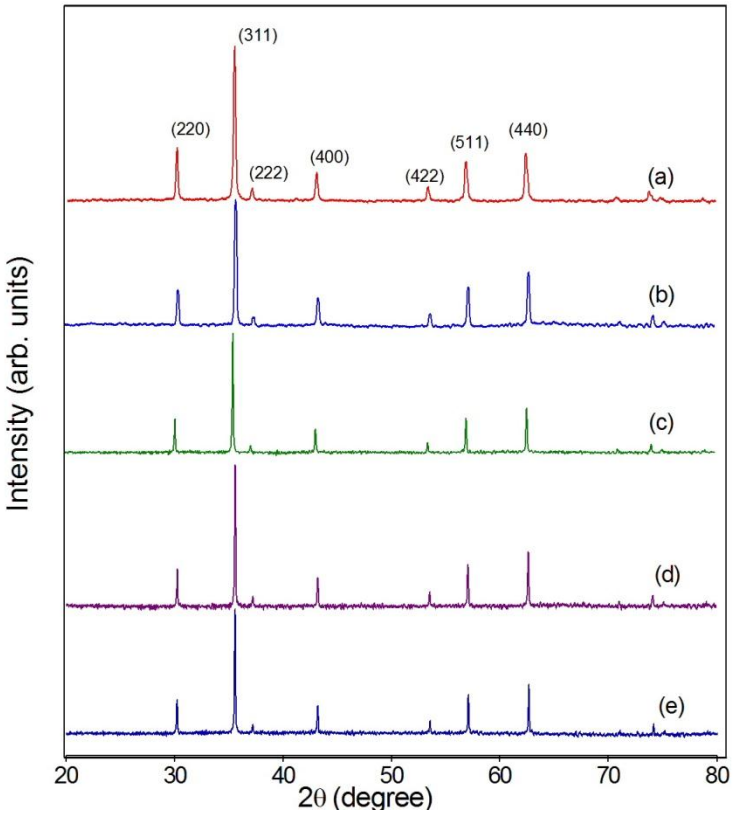

Fig.1 X-ray powder diffraction for $Co_{0.5}Zn_{0.5-x}Cu_xFe_2O_4$ samples (a) x=0.0, (b) x=0.1, (c) x=0.2 (d) x=0.3 and (e) x=0.4

The formation of single spinel phase was confirmed by comparing X-ray diffraction lines corresponding to (220), (311), (222), (400), (422), (511) and (440) planes with standard diffraction plot (Co ferrite 22-1086 ICDD and Zn ferrite 89-1009 ICDD). It is interesting to observe that broadness of diffracted peaks decreases with increasing Cu concentration, which implies the influence of Cu on crystallite size. The lattice constant "a_o" calculated using the following equation

$$a_o = d\sqrt{h^2 + k^2 + l^2} \qquad (1)$$

where 'd' is the interplanar spacing and (hkl) is the miller index of the XRD reflection peak.

Fig. 2 shows the variation of lattice constant with Cu^{2+} ion concentration. It is clear from fig. 2 that lattice constant decreases with increase in Cu^{2+} content. The observed decrease in lattice constant is in accordance with Vegard's law [11].

International Journal of Engineering Research & Technology (IJERT)
ISSN: 2278-0181
Vol. 6 Issue 01, January-2017

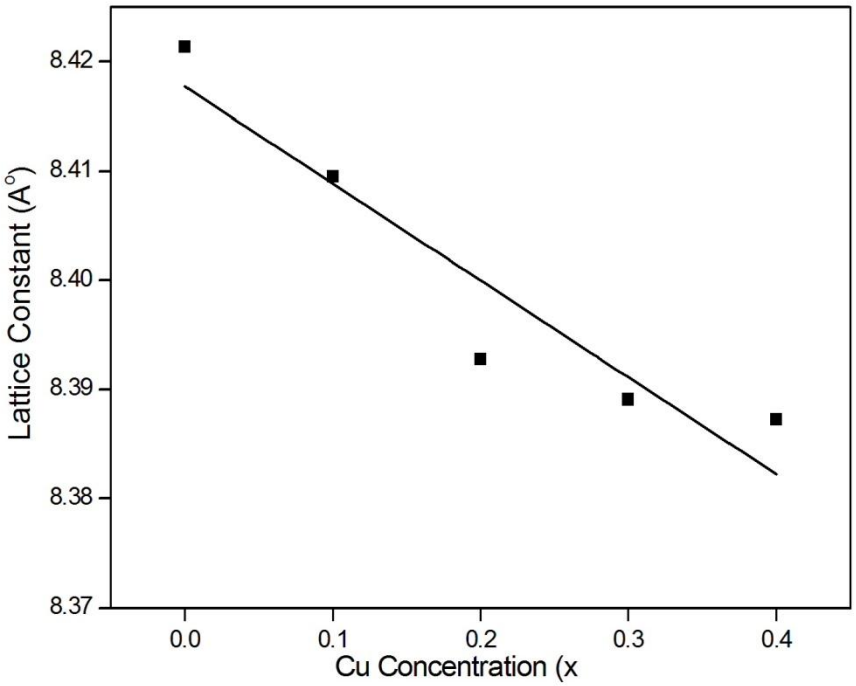

Fig.2 lattice constant 'a_o' of $Co_{0.5}Zn_{0.5-x}Cu_xFe_2O_4$ samples as a function of Cu concentration (x)

The lattice constant of pure $Co_{0.5}Zn_{0.5}Fe_2O_4$ 8.4214 Å±0.002Å, which is in good agreement with the earlier reported values [12-13]. The observed decrease in lattice constant is primarily due to difference in the ionic radii of Cu^{2+} (0.72 Å) and Zn^{2+} (0.83 Å). In the present series, $Co_{0.5}Zn_{0.5-x}Cu_xFe_2O_4$ system, it is well reported that Zn^{2+} ions have preference to occupy tetrahedral (A) sites, Co^{2+} ions have marked preference to occupy B sites in spinel lattice. Thus the smaller Cu^{2+} ions replaces the larger Zn^{2+} ions, results in the observed decrease in lattice constant with increasing Cu^{2+} content. However, a monotonic decrease is not observed, which is due to the difference in the occupancy ratio of Cu ions in A and B sublattices.

The observed broadness in the diffraction peaks (Fig. 1) indicates nano crystalline nature of the samples. As is clear from a visual inspection of XRD pattern, broadening decreases with increasing Cu content. Assuming the broadening comes only from crystallite size, we used Scherrer formula to get the crystallite size [14]

$$D_{311} = \frac{0.9\lambda}{\beta\cos\theta} \qquad (3)$$

where D_{311}, λ, β and θ are volume-averaged crystallite size, wavelength of X-ray (1.5406Å), full width at half maximum of (311) peak and diffraction angle respectively. The lattice parameter, average crystallite size estimated from Scherrer method for all the samples are listed in Table 1.

Table 1 Lattice constant (a_o), theoretical lattice constant (a_{th}), Crystallite size (D_{311}) and particle size (t) of $Co_{0.5}Zn_{0.5-x}Cu_xFe_2O_4$ samples

Cu concentration (x)	a_o (Å)	a_{th} (Å)	D_{311} (nm)
0.0	8.4269	8.4213	51
0.1	8.4218	8.4095	34.9
0.2	8.4167	8.3927	84
0.3	8.4117	8.3891	90
0.4	8.4073	8.3872	100

International Journal of Engineering Research & Technology (IJERT)
ISSN: 2278-0181
Vol. 6 Issue 01, January-2017

A measurable progressive increase in crystallite size with Cu^{2+} concentration is observed. The increase in crystallite size affects the cation distribution, which in turn modifies the properties of the ferrites drastically. In general, crystal growth depends on various parameter is like molecular concentration, temperature, heat treatment (temperature promotes crystallization due to the atomic mobility, reduction of structural defects and dislocations), site preferences and electronic configuration. In Co-Zn ferrite, Zn^{2+} ions have a very strong preference for tetrahedral sites, Co^{2+} ions have a preference for octahedral site and Fe^{3+} ions have a preference for both octahedral and tetrahedral sites. The substitution of Cu^{2+} amongst the different sites modifies the Fe^{3+} concentration at octahedral and tetrahedral site. Thus the cationic preferences are not fully satisfied due to the substitution of Cu^{2+}, which causes the increase in crystallite size [15].

3.2 X-ray and bulk density

The bulk density 'd_b' of each sample was measured using Archimedes principle and x-ray density 'd_x' was determined using the well know relation [16]

$$d_x = \frac{ZM}{Na_0^3} \qquad (5)$$

where M is molecular weight of the particular ferrite, N is Avogadro's number, a_o is experimental lattice constant and Z is number of molecules per unit cell i.e. 8 (In spinel lattice each primitive unit cell contains eight molecules). The variation of 'd_x' and 'd_b' with Cu content is shown in Fig. 3.

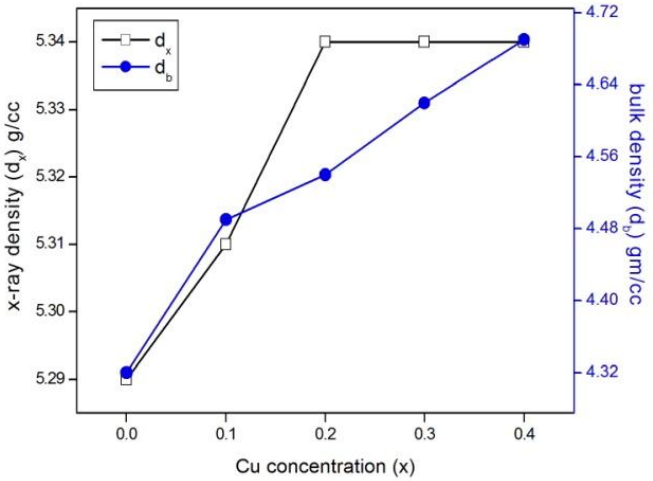

Fig.3 x-ray and bulk density $Co_{0.5}Zn_{0.5-x}Cu_xFe_2O_4$ samples as a function of Cu concentration (x)

In general, bulk density is lower than x-ray density i.e. $d_b<d_x$ because of the formation of pores during sintering process. It is clear from fig 3 that 'd_x' and 'd_b' increases with the increase in Cu^{2+} concentration. The increase in d_x is a direct consequence of decrease in lattice constant 'a_o', since the difference in ionic radii of constitute ions, causing decrease in lattice constant. In case of 'd_b' the increase is due to the difference in the densities of Cu (8.95g/cc) and Zn (7.13g/cc).

3.3 Cation distribution

The distribution of cations among A and B sites was estimated from the analysis of X-ray line intensities adopted from Buerger method [17]. According to this method the calculated (theoretical) values of intensity ratios between a pair of diffraction lines/planes (220), (400) and (422) were compared with the experimentally observed ones. This is due to the fact that, the intensity of x-ray diffraction lines depends on cations present in the tetrahedral and octahedral sites. Any modification in the distribution of cations causes a change in the intensity of corresponding x-ray line. It is well known that the intensities of (220) and (422) planes are sensitive to the cations located in tetrahedral (A) and octahedral (B) sites, while (400) plane intensity depends on cations in both A and B sites [14]. The proposed cation distribution over tetrahedral (A) and octahedral (B) sites and intensity ratios are summarized in Table 2.

International Journal of Engineering Research & Technology (IJERT)
ISSN: 2278-0181
Vol. 6 Issue 01, January-2017

Table 2 Intensity ratios and cation distribution in $Co_{0.5}Zn_{0.5-x}Cu_xFe_2O_4$ samples

Cu concentration (x)	I_{220}/I_{400} Cal.	I_{400}/I_{422} Cal.	I_{220}/I_{400} Expt.	I_{400}/I_{422} Expt.	A site	B Site
0.0	0.697	0.732	0.748	0.821	$Zn^{2}{}_{+0.5}\ Fe^{3+}{}_{0.5}$	$Co^{2+}{}_{0.5}Fe^{3+}{}_{1.5}$
0.1	0.684	0.468	0.782	0.446	$Zn^{2+}{}_{0.4}Cu^{2+}{}_{0.05}Fe^{3+}{}_{0.55}$	$Co^{2+}{}_{0.5}\ Cu^{2+}{}_{0.05}Fe^{3+}{}_{1.45}$
0.2	0.685	0.461	0.706	0.449	$Zn^{2+}{}_{0.3}\ Cu^{2+}{}_{0.1}\ Fe^{3+}{}_{0.6}$	$Co^{2+}{}_{0.5}\ Cu^{2+}{}_{0.1}Fe^{3+}{}_{1.4}$
0.3	0.689	0.478	0.757	0.513	$Zn^{2+}{}_{0.2}Co^{2+}{}_{0.08}Cu^{2+}{}_{0.12}Fe^{3+}{}_{0.6}$	$Co^{2+}{}_{0.42}\ Cu^{2+}{}_{0.18}\ Fe^{3+}{}_{1.4}$
0.4	0.686	0.476	0.826	0.479	$Zn^{2+}{}_{0.1}Co^{2+}{}_{0.2}Cu^{2+}{}_{0.18}Fe^{3+}{}_{0.52}$	$Co^{2+}{}_{0.3}Cu^{2+}{}_{0.22}Fe^{3+}{}_{1.48}$

It is found that the experimental and calculated intensities are consistent with each other. It can be seen that both Zn^{2+}, Co^{2+} ions preferentially occupy A and B sites respectively and Fe^{3+} ions are distributed in to both A and B sites for x=0.0. With increasing Cu^{2+} content (x>0.0), a fraction of Cu^{2+} ions enter in to A sites though they had large preference energy for octahedral site. It is especially observed when x>0.2, a fraction of Co^{2+} ions migrated in to tetrahedral (A) site. The proposed cation distribution also supports the changes in magnetic properties.

In order to ensure the correctness of proposed cation distribution mean ionic radii of A, B sites and theoretical lattice parameter 'a_{th}' were calculated using the following relation [18]

$$a_{th} = \frac{8}{3\sqrt{3}}\left[(r_A + R_0) + \sqrt{3}(r_B + R_0)\right] \qquad (6)$$

where r_A and r_B are the radii of tetrahedral site (A) and octahedral (B) site, R_o is the radius of oxygen.. Theoretical lattice constant values are listed in Table 1. It is clear that lattice constant decreases from 8.4269Å (x=0.0) to 8.4077 Å (x=0.4), which follows the same trend as that of experimental lattice constant 'a_o'.

3.5 Microstructure

SEM images of all the samples x=0.0,0.2 and 0.4 are shown in Fig. 4. It can be seen that there are visible changes in the microstructure with increasing the Cu concentration. The grain size increased with increasing Cu concentration and there is a corresponding increase in the density of the samples. Fig. 4d represents the Energy Dispersive x-ray spectroscopy of $Co_{0.5}Zn_{0.5}Fe_2O_4$ sample. The presence of Co, Zn and Fe are depicted in the spectra. The analysis suggest that expected stoichiometry was maintained in the sample.

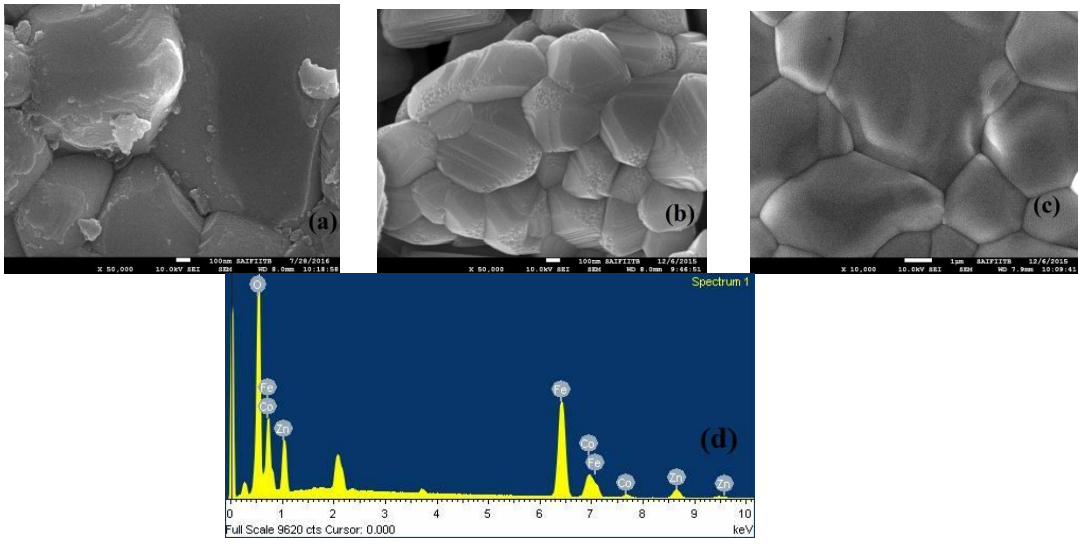

Fig.4 SEM micrographs of $Co_{0.5}Zn_{0.5-x}Cu_xFe_2O_4$ samples as a function of Cu concentration (x) (a) x=0.0 (b) x=0.2 (c) x=0.4 and (d) EDS of x=0.0

3.2 Magnetic Properties

Room temperature (300K) hysteresis loops of $Co_{0.5}Zn_{0.5-x}Cu_xFe_2O_4$ samples in the applied field of range -10 to +10 kOe are shown in Fig 5. Saturation magnetization (M_s), Coercivity (H_c) and remanent magnetization (M_r) are calculated using these plots and listed in Table 5. In the present work, saturation magnetization of undoped $Co_{0.5}Zn_{0.5}Fe_2O_4$ is significantly improved over the earlier reported values [2, 12-13,19-20].

International Journal of Engineering Research & Technology (IJERT)
ISSN: 2278-0181
Vol. 6 Issue 01, January-2017

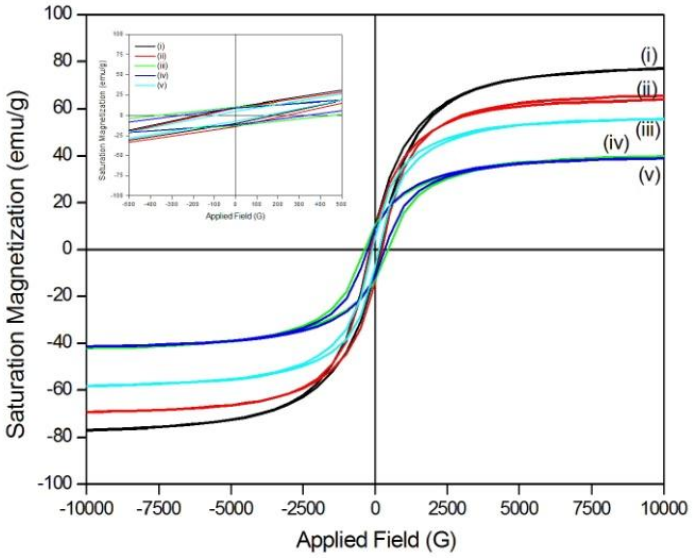

Fig.5 Magnetization curves of $Co_{0.5}Zn_{0.5-x}Cu_xFe_2O_4$ samples as a function of Cu concentration (x) (i) x=0.0 (ii) x=0.1 (iii) x=0.2 (iv) x=0.3 (v) x=0.4. Inset at left side top corner shows coercive fields.

The magnetic moment (μ_B) for Cu^{2+}, Co^{2+},Fe^{3+} and Zn^{2+} are 1,3,5 and 0μ_B respectively. Thus one can expect that an increase in magnetization with increasing Cu content because non-magnetic Zn^{2+} (0μ_B) ions are replaced by magnetic Cu^{2+}(1μ_B) ions. In contrast to above a non linear variation was observed in the present case. Saturation magnetization (M_s) decreases form 90.71 (x=0.0) to 40 emu/g (x=0.2) and increased to 57 emu/g for x=0.4, with increasing Cu^{2+} ion content.

In general, saturation magnetization depends not only on the density of cations among the sub-lattices A and B but also their direction of orientation. In ferromagnetic materials tetrahedral (A) and octahedral (B) sublattices are spontaneously magnetized and aligned in a direction opposite to each other. Thus, the net magnetization can be represented as $|M|=|M_B-M_A|$, where M_A, M_B magnetization of sublattices A and B, respectively. Any change in the cation distribution is a direct consequence of method of processing, sintering temperature and particle size. The simultaneous distribution of magnetic Cu^{2+} ions in A (in place of non-magnetic Zn^{2+} ions) and B sites causes observed non-linear variation in magnetization. From Table 2, it can be seen that Cu^{2+} ions distributed in to both A and B sites. When Cu ions occupy B-site, some of the Fe^{3+} ions are migrated in to A-site. This causes an increase in the magnetization of A sublattice due to the difference in the magnetic moments of Cu^{1+} (1μ_B) and Fe^{3+} (5μ_B) ions. Therefore, the net magnetization (M) decreases up to x=0.3. Further the increase in magnetization for x=0.4, is due to the migration of Co^{2+} ions in to A-sites.

The theoretical ($\mu_{Bth.}$)and observed ($\mu_{Bobs.}$) Bohr magnetons were calculated using the following equations:

$$\mu_{Bth} = M_B(x) - M_A(x)\ \mu_{Bobs.} = \frac{(M.Wt\ X\ M_S)}{5585} \qquad (8)$$

where $M_B(x)$, $M_A(x)$ are magnetic moments of B and A sites respectively. M_s and M.Wt are saturation magnetization and molecular weight of the sample. The calculated values with respect to Cu composition are presented in Table 3.

International Journal of Engineering Research & Technology (IJERT)
ISSN: 2278-0181
Vol. 6 Issue 01, January-2017

Table 3 Saturation magnetization (M_s), remanent magnetization (M_r), Coercivity (H_c), experimental and theoretical Bohr magneton (μ) $Co_{0.5}Zn_{0.5-x}Cu_xFe_2O_4$ samples

Concentration (x)	M_s (emu/g)	M_r (emu/g)	H_c (Oe)	$\mu_{Bobs.}$	$\mu_{Bth.}$
	90.7	11.7	177.8	3.9	6.5
0.1	67.5	11.6	198.9	2.9	6
0.2	41	11.8	408.3	1.7	5.5
0.3	40.2	10.4	298.5	1.7	5.08
0.4	57	6.3	120.2	2.4	5.14

The inset in fig.5 corresponds to the variation of coercive field with Cu content. As seen from Table 5, H_c increases initially (177.8Oe , x=0.0) and reaches to a maximum value 408Oe (x=0.2) and then decreases to 120 Oe (x=0.5). It is well known that grain size, cation distribution, magnetocrystalline anisotropy and saturation magnetization affects the coercive field. The strong magnetocrystalline anisotropy of the octahedral Co^{2+} ions enhance Coercivity. Furthermore, the migration of cobalt from B to A sites reduces the anisotropy of B sites, which in turn decreases Hc.

4 CONCLUSIONS

The main conclusions that may be derived from the obtained results are: Sol-gel combustion method effectively produce single phase and nano crystalline Co-Zn ferrite within short duration of time without any secondary phase. The decrease lattice constant confirms the solubility of Cu^{2+} ions in the spinel lattice. Density, and grain size are affected by the substitution of Cu ions. Magnetic measurements shows that saturation magnetization of $Co_{0.5}Zn_{0.5}Fe_2O_4$ is higher than that of reported values. The redistribution of cations and existence of spin canting between A and B sublattices reduces the saturation magnetization. These samples are useful in magnetic recording applications, because recording media requires a high saturation magnetization and a moderately high Coercivity.

REFERENCES

[1] M Stefanescu, M Bozdog, C Muntean, O Stefanescu, T Valse J. Magn.Magn. Mater. 393 92-98 (2015)
[2] A Franco, Jr. and F.C.e Silva Effect J. Appl. Phys 113, 17B513 (2013)
[3] D Birajhdar S E Shirsath R H Kadam, J Sol-Gel Sci. Tech. 58, 70-79 (2011)
[4] A V Raut, R S Barkule, D R Shengule, K M Jadhav J. Magn. Magn. Mater. 358-359, 87-92 (2014)
[5] T Abraham, Am. Ceram. Soc. Bull. 73 62-65 (1994)
[6] S. K. Banerjee, P. D. Baba, B. J. Evans, and S. S. Hafner, J. Phys. (France) 32, 1971, Cl-145-147
[7] W Ling, H Zhong Ying He, Yang Wu, K Yang, Yuanxum Li, Sheng Li, J. Magn.Magn.Mater. 322, 819-823 (2011)
[8] M C Dimri, A K Verma, S C Kashyap, D C Dube and O P Thakur, Mat. Sci and Engg. B 133, 42-48 (2006)
[9] V K Lakhani and K B Modi, J. Phys. D. Appl. Phys. 44, 245403 (2011)
[10] JB Nelson and DP Riley Proc. Phys. Soc. 57, 477 (1945)
[11] A.R.Denton and N W Aschroft, Phys. Rev. A 43, 3161 (1991)
[12] S S Jadhav, S E Shirsath, Sunil M P and K M Jadav, J. Appl. Phys. 108, 093920 (2010)
[13] I Sharifi, H Shokrollahi J.Magn. Magn. Mater. 324, 2397-2403 (2012)
[14] B.D. Cullity "Elements of X-ray diffraction", Philippines, Addison Wesley Publishing Company, Inc., 2nd Edition. California, 1978.
[15] S.A. Chandana Rath, R.P. Das, K.K. Sahu, S.D. Kulkarni, J. of Appl. Phys. 91 (2002) 2211
[16] B. Rajesh Babu, M.S.R. Prasad, K.V. Ramesh, Y. Purushotham, Mater. Chem. and Phys. 148, 585-591 (2014)
[17] M.J. Buerger "Crystal Structure Analysis" Wiley, New York, 1960
[18] B. Rajesh Babu, M. S. R. Prasad and K. V. Ramesh, Inter. J. of Mod. Phys. B. 29, 1550032 (2015)
[19] R Arulmurugan, B Jeyadevan, G Vaidyanathan, S Sendhilnathan, J. Magn.Magn.Mater. 288, 470-477 (2005)
[20] D.S. Nikam, S V Jadhav, V M Khot, M R Phadatare, S H Pawar, J. Magn.Magn.Mater 349, 208-213 (2014)